Quark deconfinement transition in neutron stars with the field correlator method

Domenico Logoteta [1] and Ignazio Bombaci [2]
[1] *Centro de Física Computacional, Department of Physics, University of Coimbra, 3004-516 Coimbra, Portugal and*
[2] *Dipartimento di Fisica "Enrico Fermi", Universitá di Pisa, and INFN Sezione di Pisa, Largo Bruno Pontecorvo 3, I-56127 Pisa, Italy*
(Received 21 May 2013; accepted 19 August 2013)

A phase of strong interacting matter with deconfined quarks is expected in the core of massive neutron stars. In this article, we perform a study of the hadron-quark phase transition in cold ($T = 0$) neutron star matter and we calculate various structural properties of hybrid stars. For the quark phase, we make use of an equation of state (EOS) derived with the field correlator method (FCM) recently extended to the case of nonzero baryon density. For the hadronic phase, we consider both pure nucleonic and hyperonic matter, and we derive the corresponding EOS within a relativistic mean field approach. We make use of measured neutron star masses, and particularly the mass $M = 1.97 \pm 0.04\, M_\odot$ of PSR J1614-2230 to constrain the values of the gluon condensate G_2, which is one of the EOS parameters within the FCM. We find that the values of G_2 extracted from the mass measurement of PSR J1614-2230 are consistent with the values of the same quantity derived within the FCM from recent lattice QCD calculations of the deconfinement transition temperature at zero baryon chemical potential. The FCM thus provides a powerful tool to link numerical calculations of QCD on a space-time lattice with measured neutron star masses.

PACS numbers: 97.60.Jd, 21.65.+f, 12.38.Aw, 12.38.Mh

arXiv:1309.0096v1 [nucl-th] 31 Aug 2013

I. INTRODUCTION

Neutron stars contain in their interiors one of the densest form of matter in the Universe. In fact, neutron star structure calculations [1–4] based on a large variety of modern equations of state of dense hadronic matter predict a maximum stellar central density (the one for the maximum mass star configuration) in the range of 4 – 8 times the saturation density ($\sim 2.8 \times 10^{14}$ g/cm^3) of nuclear matter. Thus these stars can be viewed as natural laboratories to explore the low-temperature T and high baryon chemical potential region of the phase diagram of quantum chromodynamics (QCD) [5–8]. In this regime nonperturbative aspects of QCD are expected to play a crucial role, and a transition to a phase with deconfined quarks and gluons is expected to occur and to influence a number of interesting astrophysical phenomena [9–16].

Recent high-precision numerical calculations of QCD on a space-time lattice at zero baryon chemical potential μ_b (zero baryon density) have shown that at high temperature and for physical values of the quark masses, the transition to quark gluon plasma is a crossover [17–19] rather than a real phase transition.

Unfortunately, present lattice QCD calculations at finite baryon chemical potential are plagued with the notorious "sign problem", which makes them unrealizable by all presently known lattice methods (see e.g. [20] and references therein). Thus, to explore the QCD phase diagram at low-temperature T and high μ_b, it is necessary to invoke some approximations in QCD or to apply a QCD effective model.

Along these lines, for example, a model of the equation of state (EOS) of quark matter [21] inspired by the MIT bag model of hadrons [22] has been intensively used by many authors to calculate the structure of strange stars [23–27], or the structure of the so-called hybrid stars, i.e. neutron stars with a quark matter core. In this model quark matter is treated as a free relativistic Fermi gas of u, d and s quarks, which reside in a region characterized by a constant energy density B, with at most perturbative corrections up to the second order in the QCD structure constant α_s [28–30]. The parameter B takes into account, in a crude phenomenological manner, nonperturbative aspects of QCD and it is related to the bag constant which in the MIT bag model [22] gives the confinement of quarks within hadrons. The bag model EOS is expected to be reasonable at asymptotically large density, but it crumbles in the density region where quarks clusterize to form hadrons, i.e. in the region where the deconfinement phase transition takes place.

Another very used quark model is the Nambu–Jona-Lasinio (NJL) model [31] (for a thorough review see [32]). This model has proved to be very successful in the description of the spontaneous breakdown of chiral symmetry exhibited by true QCD vacuum. It explains very well the spectrum of the low-lying mesons as well as many other low-energy phenomena of strong interaction [33–35]. The NJL is not a confining model and it is based on an effective chiral Lagrangian that captures some of symmetries of QCD. In the NJL approach quarks interact each other through a nonrenormalizable pointlike Fermi interaction. The entire system is gluon free so it cannot be used in the limit of low density and high temperature.

In the case of the MIT bag model a large window of the parameters allows for the existence of stable strange stars or hybrid stars. In the case of the NJL model the existence of stable hybrid stars is very unlikely [36] or is

possible only for a restricted range of the model parameters [37–40].

As we have commented, the MIT bag model and the NJL model (as other QCD effective models) cannot make predictions in the high-T and zero baryon chemical potential region, and thus cannot be tested using present lattice QCD calculations.

Recently the deconfinement phase transition has been described using an EOS of quark gluon plasma derived within the field correlator method (FCM) [41, 42] extended to finite baryon chemical potential [43–46]. The field correlator method is a nonperturbative approach to QCD which includes from first principles the dynamics of confinement in terms of color electric and color magnetic correlators. The model is parametrized in terms of the gluon condensate G_2 and the large-distance static quark-antiquark ($Q\bar{Q}$) potential V_1. These two quantities control the EOS of the deconfined phase at fixed quark masses and temperature. The main constructive characteristic of the FCM is the possibility to describe the whole QCD phase diagram as it can span from high temperature and low baryon chemical potential, to low T and high μ_b limit.

A very interesting feature of the FCM is that the value of the gluon condensate can be obtained from lattice QCD calculations [47, 48] of the deconfinement transition temperature T_c, at zero baryon chemical potential. Thus we have an efficacious tool to directly link lattice simulations and neutron star physics.

To explore this link is one of the main purposes of the present work. In particular, we will investigate the possibility for the occurrence of the quark deconfinement transition in neutron stars and the possibility to have stable hybrid star configurations using the field correlator method for the quark phase EOS and a relativistic mean field model [49, 50] for the EOS of the hadronic phase. A similar study has been performed in Ref. [51], where a microscopic EOS derived with the Brueckner-Hartree-Fock approximation [52–54] has been employed to describe the hadronic phase, whereas, for the quark phase, the FCM has been used as in the present work. The properties of absolutely stable [23] strange quark matter and strange stars have been recently investigated within the FCM by the author of Ref. [55].

This work is organized as follows: In Sec. II we briefly review the FCM at finite temperature and density; in Secs. III and IV we discuss respectively the hadronic EOS and the formalism of phase transition to quark matter in β-stable hadronic matter; our main results are presented in Sec. V; the link between lattice QCD calculations and measured neutron star masses is discussed in Sec. VI; finally the conclusions of this work are outlined in Sec. VII.

II. EOS OF THE QUARK PHASE

The quark matter equation of state we used in the present work is based on the FCM [41] (see [42]for a detailed review). Recently this method has been extended to the case of nonzero baryon density [43–46] making possible its application to neutron star matter.
The principal advantage of the FCM is a natural explanation and treatment of the dynamics of confinement in terms of color electric $D^E(x)$, $D_1^E(x)$ and color magnetic $D^H(x)$, $D_1^H(x)$ Gaussian correlators.

The correlators $D^E(x)$, $D_1^E(x)$ and $D^H(x)$, $D_1^H(x)$ are related to the nontrivial two-point correlation function for the color electric and color magnetic fields [42].
D^E contributes to the standard string tension σ^E through [43]

$$\sigma^E = \frac{1}{2}\int D^E(x)\; d^2x. \tag{1}$$

The string tension σ^E vanishes as D^E goes to zero at $T \geq T_c$ and this leads to deconfinement. The correlators have been calculated on the lattice [56–58] and also analytically [59].

In the lowest nonperturbative approximation one can hold only single quark and gluon interactions with the vacuum. This is the so-called called single line approximation [43]. Using this approximation the quark pressure P_q for a single flavor, reads [43, 45, 46]

$$P_q/T^4 = \frac{1}{\pi^2}[\phi_\nu(\frac{\mu_q - V_1/2}{T}) + \phi_\nu(-\frac{\mu_q + V_1/2}{T})] \tag{2}$$

where

$$\phi_\nu(a) = \int_0^\infty du \frac{u^4}{\sqrt{u^2+\nu^2}} \frac{1}{\exp\left[\sqrt{u^2+\nu^2} - a\right] + 1}\,, \tag{3}$$

$\nu = m_q/T$ and V_1 is the large-distance static $Q\bar{Q}$ potential:

$$V_1 = \int_0^{1/T} d\tau(1-\tau T)\int_0^\infty d\chi\chi D_1^E(\sqrt{\chi^2+\tau^2})\,. \tag{4}$$

The nonperturbative contribution to $D_1^E(x)$ is parametrized as [42]

$$D_1^E(x) = D_1^E(0)\exp(-|x|/\lambda) \tag{5}$$

where λ is the vacuum correlation length. Following Ref. [43], we use the value $\lambda = 0.34$ fm which has been determined in lattice QCD calculations [57].

In this formalism V_1 in Eq.(4) is independent on the chemical potential (and so on the density). This feature is partially supported by lattice simulations at small chemical potential [43, 60]. In the present work, the value of V_1 at $T = 0$ has been considered as a model parameter [51, 55].

The gluon contribution to the pressure is [46]

$$P_g/T^4 = \frac{8}{3\pi^2}\int_0^\infty d\chi\chi^3 \frac{1}{\exp\left(\chi + \frac{9V_1}{8T}\right) - 1}\,. \tag{6}$$

In summary the total pressure of the quark phase is given by

$$P_{qg} = P_g + \sum_{u,d,s} P_q - \frac{9}{64} G_2 \,. \tag{7}$$

The last term in Eq.(7) represents the vacuum energy difference between the quark and hadronic phases, in the case of three-flavor (u, d, s) quark matter [43], and G_2 is the gluon condensate. The latter quantity has been determined using QCD sum rules [61] to be in the range $G_2 = (0.012 \pm 0.006)$ GeV^4. In the present work, following [43–46], we assume that the gluon condensate is independent on the baryon chemical potential, and we consider the value of G_2 as a model parameter.

Notice that the quark pressure given in Eqs. (2)–(5) is the one of a relativistic ideal Fermi gas, which in the case of $T = 0$ can be written as

$$P_q = \frac{1}{4\pi^2}\left\{ k_{F,q}^3 \sqrt{k_{F,q}^2 + m_q^2} - \frac{3}{2}\, m_q^2 \left[k_{F,q} \sqrt{k_{F,q}^2 + m_q^2} - m_q^2 \, \ln\left(\frac{k_{F,q} + \sqrt{k_{F,q}^2 + m_q^2}}{m_q} \right) \right] \right\} , \tag{8}$$

where the Fermi momentum $k_{F,q}$ is related to the chemical potential μ_q of quarks with flavor q by

$$\mu_q = \sqrt{k_{F,q}^2 + m_q^2} + \frac{V_1}{2} \,. \tag{9}$$

The energy density ε_q at $T = 0$ can be obtained using Eq.(8) and the thermodynamical relation

$$\varepsilon_q = -P_q + \mu_q \, n_q \,, \tag{10}$$

where $n_q = \frac{1}{\pi^2} \, k_{F,q}^3$ is the number density for quarks with flavor q.
One thus obtains the energy density of a relativistic ideal Fermi gas plus an extra term

$$\varepsilon_q' = \frac{V_1}{2} \, \frac{k_{F,q}^3}{\pi^2} \tag{11}$$

which originates from the large-distance static $Q\bar{Q}$ potential $V_1 \equiv V_1(T = 0)$.

In our calculations we used the following values of the current-quark masses: $m_u = m_d = 5$ MeV and $m_s = 150$ MeV.

In summary, the EOS for the quark gluon phase has two parameters: G_2 and $V_1 \equiv V_1(T = 0)$.

In the present work we have not considered the possibility of color superconductivity (see e.g. [5] and references therein). As discussed in [44, 62] the low-temperature deconfinement transition produces a strong nonperturbative attraction in colorless channels that results in a dominance of the $Q\bar{Q}$ correlations over the diquark QQ ones. Thus within the FCM, QQ pairing and possible phases of color superconducting quark matter are hardly possible [44, 62].

III. EOS OF THE HADRONIC PHASE

We adopt a nonlinear relativistic mean field model [49, 50] for the EOS of hadronic matter and we make use of the parametrization GM1 given by Glendenning and Moszkowski [63, 64]. The Lagrangian density including the baryonic octet, in terms of scalar σ, the vector-isoscalar ω_μ, and the vector-isovector $\vec{\rho_\mu}$ meson fields, reads

$$\mathscr{L} = \mathscr{L}_{hadrons} + \mathscr{L}_{leptons} \,, \tag{12}$$

where the hadronic contribution is

$$\mathscr{L}_{hadrons} = \mathscr{L}_{baryons} + \mathscr{L}_{mesons} \,, \tag{13}$$

with

$$\mathscr{L}_{baryons} = \sum_{baryons} \bar{\Psi}_B [\gamma^\mu D_\mu - M_B^*] \Psi_B \,, \tag{14}$$

where

$$D_\mu = i\partial_\mu - g_{\omega B}\omega_\mu - g_{\rho B}\vec{t}_B \cdot \vec{\rho}_\mu \,, \tag{15}$$

and $M_B^* = M_B - g_{\sigma B}\sigma$. The quantity $\vec{t}_B$ designates the isospin of baryon B. The mesonic contribution reads

$$\mathscr{L}_{mesons} = \mathscr{L}_\sigma + \mathscr{L}_\rho + \mathscr{L}_\omega \,, \tag{16}$$

with

$$\mathscr{L}_\sigma = \frac{1}{2}(\partial_\mu\sigma\partial^\mu\sigma - m_\sigma^2) + \frac{1}{3!}\kappa\sigma^3 + \frac{1}{4!}\lambda\sigma^4 \,, \tag{17}$$

$$\mathscr{L}_\omega = -\frac{1}{4}\Omega_{\mu\nu}\Omega^{\mu\nu} + \frac{1}{2}m_\omega^2\omega_\mu\omega^\mu \,, \tag{18}$$

$$\Omega_{\mu\nu} = \partial_\mu\omega_\nu - \partial_\nu\omega_\mu \,, \tag{19}$$

$$\mathscr{L}_\rho = -\frac{1}{4}\vec{B}_{\mu\nu}\vec{B}^{\mu\nu} + \frac{1}{2}m_\rho^2\vec{\rho}_\mu \cdot \vec{\rho}^\mu \,, \tag{20}$$

$$\vec{B}_{\mu\nu} = \partial_\mu\vec{\rho}_\nu - \partial_\nu\vec{\rho}_\mu - g_\rho(\vec{\rho}_\mu \times \vec{\rho}_\nu) \,. \tag{21}$$

For the lepton contribution we take

$$\mathscr{L}_{leptons} = \sum_{leptons} \bar{\Psi}_l [\gamma^\mu\partial_\mu - m_l^*] \Psi_l \,, \tag{22}$$

where the sum is over electrons and muons.

We have used the parametrization of the nonlinear relativistic mean field model due to Glendenning and Moszkowski [63, 64]. The nucleon coupling constants are

fitted to the bulk properties of nuclear matter. In particular, for the GM1 parametrization [63, 64] the incompressibility of symmetric nuclear matter and the nucleon effective mass at the empirical saturation density are respectively $K = 300$ MeV and $M^* = 0.7M$ (being M the bare nucleon mass). The inclusion of hyperons involves new couplings, which can be written in terms of the nucleonic ones: $g_{\sigma Y} = x_\sigma g_\sigma$, $g_{\omega Y} = x_\omega g_\omega$ and $g_{\rho Y} = x_\rho g_\rho$. In this model it is assumed that all the hyperons in the baryon octet have the same coupling. In this work we will consider x_σ in the range of 0.6 – 0.8. In addition, following Ref. [63], we will take $x_\rho = x_\sigma$, whereas the binding energy of the Λ particle in symmetric nuclear matter, B_Λ,

$$\left(\frac{B_\Lambda}{A}\right) = -28 \text{ MeV} = x_\omega \, g_\omega \, \omega_0 - x_\sigma \, g_\sigma \sigma \qquad (23)$$

is used to determine x_ω in terms of x_σ. Notice that the case with $x_\sigma = 0.6$ produces stars with a larger hyperon population (for a given stellar gravitational mass) with respect to the case $x_\sigma = 0.8$ [64, 65]. In addition to these two parametrizations for hyperonic matter (hereafter called NY matter), we will consider the case of pure nucleonic matter (hereafter called N matter).

IV. PHASE TRANSITION IN BETA-STABLE NEUTRON STAR MATTER

The composition of neutron star matter is determined by the requirements of electric charge neutrality and equilibrium under the weak interaction processes (β-stable matter). Under such conditions, in the case of neutrino-free matter, the chemical potential μ_i of each particle species i can be written in terms of two independent quantities, the baryonic and electric chemical potentials μ_b and μ_q respectively [7],

$$\mu_i = b_i \mu_b - q_i \mu_q \ , \qquad (24)$$

where b_i is the baryon number of the species i, and q_i denotes its charge in units of the electron charge magnitude.

In the pure hadronic phase, $\mu_b = \mu_n$ is the neutron chemical potential, and $\mu_q = \mu_e$ is the electron chemical potential. In the pure quark phase the quark chemical potentials μ_f (f=u, d, s) are related to μ_b and μ_q by the formulas $\mu_u = (\mu_b - 2\mu_q)/3$ and $\mu_d = \mu_s = (\mu_b + \mu_q)/3$.

We next assume a first-order hadron-quark phase transition [66] and, following Glendenning [67], we require global electric charge neutrality of bulk β-stable stellar matter. An important consequence of imposing global charge neutrality is that the hadronic and the quark phases can coexist for a finite range of pressures. This treatment of the phase transition is known in the literature as the Gibbs construction for the mixed phase. In this case the Gibbs conditions for phase equilibrium can be written as

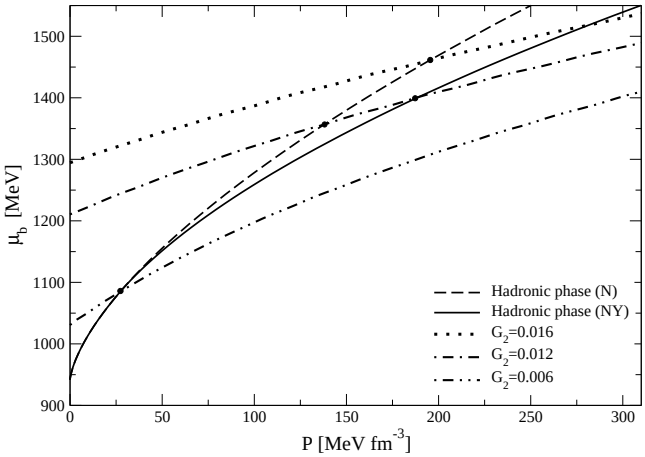


FIG. 1: Baryon chemical potential μ_b versus pressure P in cold ($T = 0$) β-stable matter. Curves for the quark phase are relative to three different values of the gluon condensate G_2 reported in GeV^4, and $V_1 = 0.01$ GeV. Curves for the hadronic phase are relative to hyperonic matter (NY) with $x_\sigma = 0.7$ and to pure nucleonic matter (N).

$$\mu_{b,H} = \mu_{b,Q} \equiv \mu_b \qquad (25)$$

$$\mu_{q,H} = \mu_{q,Q} \equiv \mu_q \qquad (26)$$

$$T_H = T_Q \equiv T \qquad (27)$$

$$P_H(\mu_b, \mu_q, T) = P_Q(\mu_b, \mu_q, T) \qquad (28)$$

With the purpose to compare with previous studies [51], we also make use of the so-called Maxwell construction for the phase transition. In this case, one imposes that each phase in equilibrium is separately charge neutral. Now the conditions for phase equilibrium can be written as

$$\mu_{b,H} = \mu_{b,Q} \equiv \mu_b \qquad (29)$$

$$T_H = T_Q \equiv T \qquad (30)$$

$$P_H(\mu_b, \mu_q(\mu_b), T) = P_Q(\mu_b, \mu_q'(\mu_b), T) \ . \qquad (31)$$

In this case the electric chemical potential $\mu_q = \mu_e$ has a discontinuity [67] at the interface between the two phases [77].

In the following we consider the case of cold (i.e. $T = 0$) matter, which is appropriate to describe neutron stars interiors at times larger than about a few minutes after their formation [7].

In Fig. 1 we plot the relation between the baryon chemical potential μ_b and the total (i.e. baryonic plus leptonic contributions) pressure P, in β-stable matter, for the hadron and the quark phases in the case of the Maxwell construction. For the hadronic phase we consider hyperonic matter (NY) with $x_\sigma = 0.7$ (continuous line) and

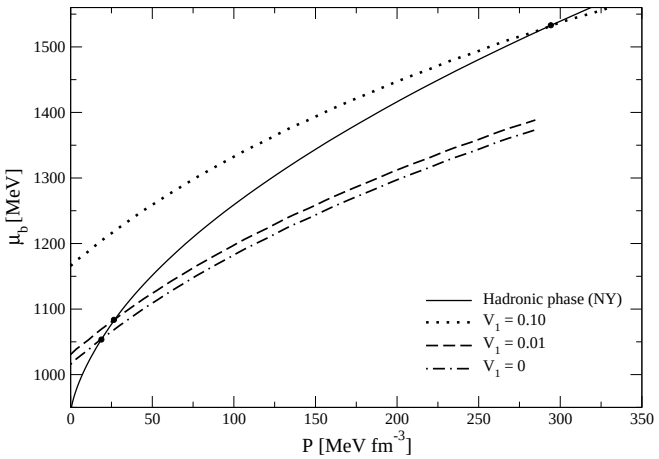


FIG. 2: Baryon chemical potential μ_b versus pressure P in cold ($T = 0$) β-stable matter. Curves for the quark phase are relative to three different values of the large-distance static $Q\bar{Q}$ potential V_1 reported in GeV, and for $G_2 = 0.006\,\mathrm{GeV}^4$. The curve for the hadronic phase is relative to hyperonic matter (NY) with $x_\sigma = 0.6$.

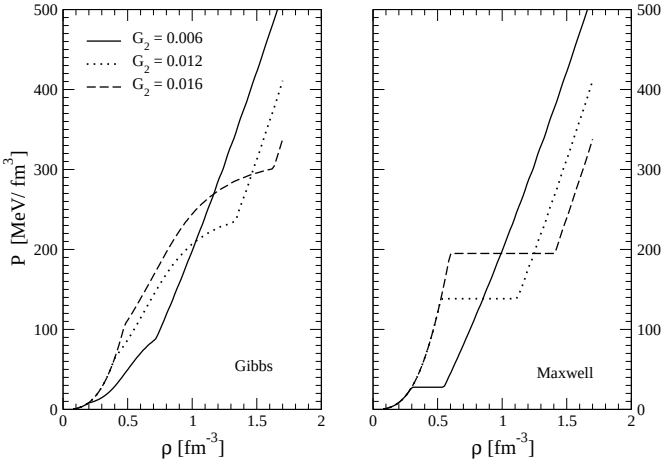


FIG. 3: Total pressure P of cold β-stable matter as a function of the baryon number density ρ, for different values of the gluon condensate G_2 (reported in GeV^4 units) and for $V_1 = 0.01\,\mathrm{GeV}$ in the case of the Gibbs (left panel) and Maxwell construction (right panel) for the phase transition. Results are relative to pure nucleonic matter (N) for the hadronic phase.

pure nucleonic matter (N) (dashed line). For the quark phase we use three different values of the gluon condensate $G_2 = 0.006$, 0.012, 0.016 GeV^4 and a common value $V_1 = 0.01\,\mathrm{GeV}$ for the large-distance static $Q\bar{Q}$ potential. The phase transition occurs at the intersection point between the curves describing the two different phases. This crossing point is significantly affected by the value of the gluon condensate, in particular when G_2 increases the onset of the deconfinement transition is shifted to higher pressure (higher baryon chemical potential). It is worthwhile to note also that the presence of hyperons in the hadronic phase moves the phase transition point to larger pressures. Similar results have been found using different values for the hyperon-nucleon couplings ($x_\sigma = 0.6, 0.8$) for the hadronic EOS.

Keeping a fixed value of the gluon condensate, $G_2 = 0.006\,\mathrm{GeV}^4$, we show in Fig. 2 the effects of V_1 on the phase transition point. As one can see, only slight differences exist between the cases $V_1 = 0$ and $V_1 = 0.01\,\mathrm{GeV}$ while for $V_1 = 0.1\,\mathrm{GeV}$ the transition point is shifted to a very high value of the pressure. This should be expected just looking at Eqs. 8 and 9, where it turns out clearly that pressure is a decreasing function of V_1.

In Figs. 3 and 4, we show the pressure for β-stable matter as a function of the baryon number density ρ in the case of pure nucleonic matter (Fig. 3) and hyperonic matter with $x_\sigma = 0.6$ (Fig. 4) for the hadronic phase. For the quark phase we consider different values of the gluon condensate G_2. Results on the left (right) panels of these two figures refer to the Gibbs (Maxwell) construction for the phase transition. As expected, the Maxwell

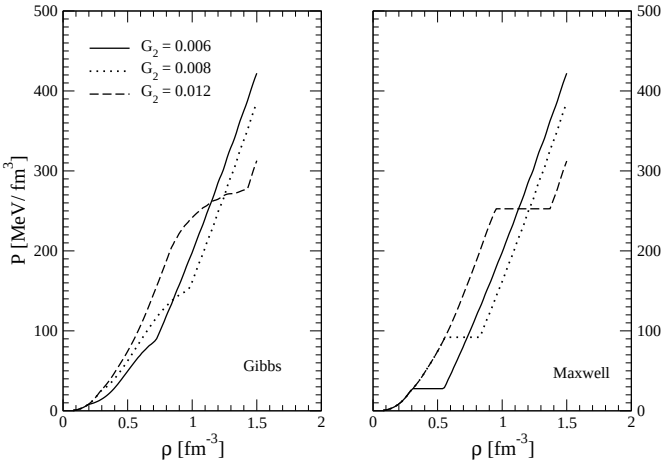


FIG. 4: Same as the previous figure, but with hyperonic matter (NY) with $x_\sigma = 0.6$ for the hadronic phase.

construction corresponds to a constant pressure in the baryon number density range of the coexistence region, whereas in the Gibbs construction the pressure increases monotonically with ρ [64, 67, 70]. Increasing the value of G_2 causes a shift of the phase transition to larger baryon densities for both the Gibbs and Maxwell constructions.

V. NEUTRON STAR STRUCTURE

In this section we show the results of our calculations of hybrid stars structure. To this purpose we integrate the well-known Tolman, Oppenheimer and Volkov relativistic hydrostatic equilibrium equations (see e.g. [64, 71]) to get various stellar properties for a fixed EOS.

We report the results of a systematic study in which we vary the value of the gluon condensate G_2 between the constraints imposed by QCD sum rules [61]. To model the neutron star crust we have used the EOS of Ref. [72].

Unless otherwise specified, all the results presented in the following have been obtained using the Gibbs construction to model the hadron-quark phase transition and taking $V_1 = 0.01\,\mathrm{GeV}$.

Let us first consider the case in which the hadronic phase does not contain hyperons, *i.e.* the case of pure nucleonic matter (N). In Fig. 5 we report the stellar gravitational mass M (in unit of the solar mass $M_\odot = 1.99 \times 10^{33}$g) versus the central baryon number density ρ_c (left panel) and the mass versus radius R (right panel) in the case of pure nucleonic stars (continuous line) and of hybrid stars for different G_2. We obtain stable hybrid star configurations for all the considered values of the gluon condensate, with maximum masses ranging from $M_{max} = 1.44\,M_\odot$ (case with $G_2 = 0.006\,\mathrm{GeV}^4$) to $M_{max} = 2.05\,M_\odot$ ($G_2 = 0.0016\,\mathrm{GeV}^4$). Notice that the hybrid star branch of the stellar equilibrium configurations shrinks as G_2 is increased. This is in full agreement with the results for the EOS reported in the left panel of Fig. 3. This behavior is different with respect to the one found by the authors of Ref. [51] where the stability window of hybrid star configurations for a nucleonic equation of state was restricted between $0.006\,\mathrm{GeV}^4 < G_2 < 0.007\,\mathrm{GeV}^4$, while no hadron-quark phase transition occurred once hyperons were included in the EOS.

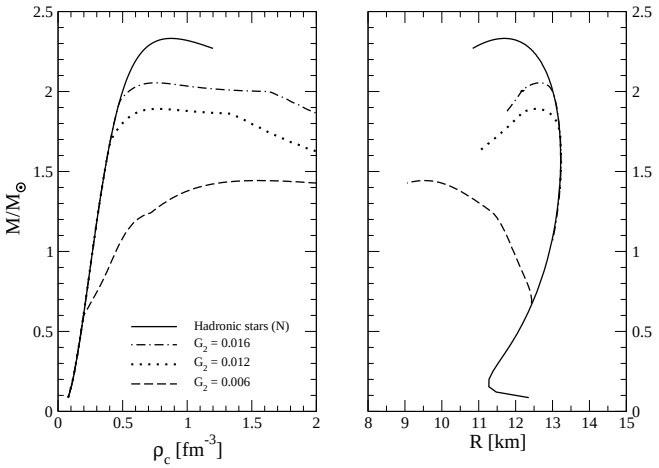


FIG. 5: Stellar gravitational mass M versus central baryon number density ρ_c (left panel) and versus stellar radius R (right panel) for hybrid stars for several values of the gluon condensate G_2 (reported in GeV^4 units) and for $V_1 = 0.01\,\mathrm{GeV}$. The continuous line in both panels refers to the pure hadronic stars (i.e. compact stars with no quark matter content). For the EOS of hadronic phase only nucleons (N) are included.

In Fig. 6 we plot the quark-hadron phase transition boundaries in β-stable matter as a function of G_2 in the case in which the hadronic phase does not contain hyperons (pure nucleonic matter). The onset of the deconfinement transition (i.e. the onset of the quark-hadron mixed phase) occurs at the baryon number density ρ_1, and the pure quark phase begins at ρ_2. Also shown is the central baryon number density ρ_c^{Hyb} of the maximum mass hybrid star (dotted-dashed line). Stable hybrid star configurations have central densities ρ_c located in the region of the ρ–G_2 plane between the dotted-dashed line and the lower continuous line, i.e. $\rho_1 < \rho_c \leqslant \rho_c^{Hyb}$. Notice that $\rho_c^{Hyb} > \rho_2$ when the gluon condensate is in the range $0.006\,\mathrm{GeV}^4 < \mathrm{G}_2 \leqslant 0.0077\,\mathrm{GeV}^4$. For these G_2 values all hybrid stars with a central density in the range $\rho_2 < \rho_c \leqslant \rho_c^{Hyb}$ possess a pure quark matter core. Finally the horizontal dashed line represents the value of the central baryon number density ρ_c^{HS} of the maximum mass pure nucleonic star.

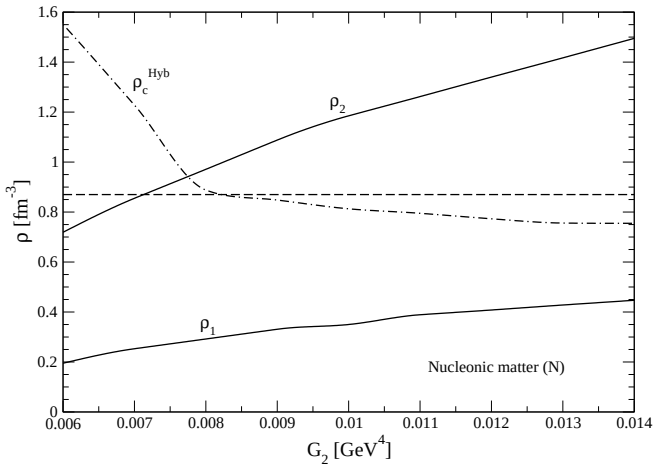


FIG. 6: Quark-hadron phase transition boundaries in β-stable matter as a function of the gluon condensate G_2 and for $V_1 = 0.01\,\mathrm{GeV}$. The onset of quark-hadron mixed phase occurs at the baryon number density ρ_1, and the pure quark phase begins at ρ_2. Also shown is the central baryon number density ρ_c^{Hyb} of the maximum mass hybrid star. The horizontal dashed line represents the value of the central baryon number density ρ_c^{HS} of the maximum mass pure hadronic star. For the EOS of hadronic phase only nucleons (N) are included.

In Fig. 7 we draw the maximum mass M_{max} for hy-

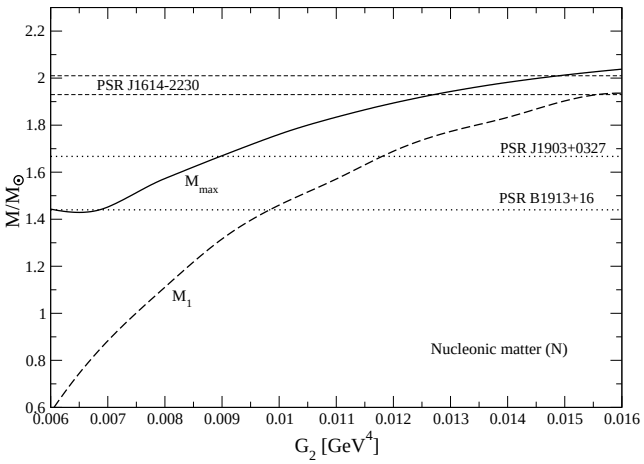


FIG. 7: Gravitational maximum mass for hybrid stars (continuous line) and gravitational mass M_1 (dashed line) of the star with central baryon number density ρ_1 corresponding to the onset of mixed quark-hadron phase as a function of the gluon condensate G_2 and for $V_1 = 0.01\,\mathrm{GeV}$. For the EOS of hadronic phase only nucleons (N) are included.

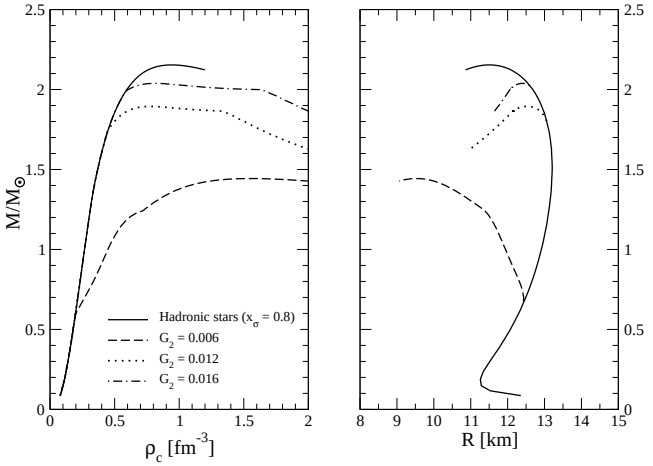


FIG. 8: Stellar gravitational mass M versus central number density ρ_c (left panel) and versus stellar radius R (right panel) for hybrid stars for several values of the gluon condensate G_2 (reported in GeV^4 units) and for $V_1 = 0.01\,\mathrm{GeV}$. The continuous line in both panels refers to the pure hadronic star sequence. The hadronic phase consists of hyperonic matter (NY) and is described by the GM1 model with $x_\sigma = 0.8$.

brid stars (continuous line) and the mass $M_1 = M(\rho_1)$ (dashed line) of the star with central baryon number density ρ_1 corresponding to the onset of the mixed phase. These two quantities are plotted as a function of the gluon condensate G_2 for the case in which the hadronic phase does not contain hyperons. Stable hybrid star configurations correspond to the region of the M–G_2 plane between the continuous and the dashed line. Stellar configurations in the region below the dashed line M_1 do not possess any deconfined quark matter in their center (nucleonic stars).

To compare our results with measured neutron star masses, we report in the same Fig. 7 the values of the masses of the following pulsars: PSR B1913+16 with $M = 1.4398 \pm 0.0002\,M_\odot$ [73], PSR J1903+0327 with $M = 1.667 \pm 0.021\,M_\odot$ [74] and PSR J1614-2230 with $M = 1.97 \pm 0.04\,M_\odot$ [75].
The mass of PSR J1614-2230 gives the strongest constraint on the possible value of the gluon condensate. In fact, using the lower bound of the measured mass of PSR J1614-2230, we get $G_2 \gtrsim 0.0129$ GeV^4. Thus for values of the gluon condensate in the range $0.0129\ \mathrm{GeV}^4 \lesssim G_2 \leqslant G_2^* \simeq 0.018\ \mathrm{GeV}^4$, PSR J1614-2230 is a hybrid star, whereas PSR B1913+16 and PSR J1903+0327 are pure nucleonic stars. In the above specified range, G_2^* is defined by the condition $M_1(G_2^*) = 2.01\ M_\odot$, the upper bound of the measured mass of PSR J1614-2230. Thus for $G_2 > G_2^*$ PSR J1614-2230 is a pure nucleonic star.

We now consider the case in which the hadronic phase contains hyperons (NY matter), and we show the results

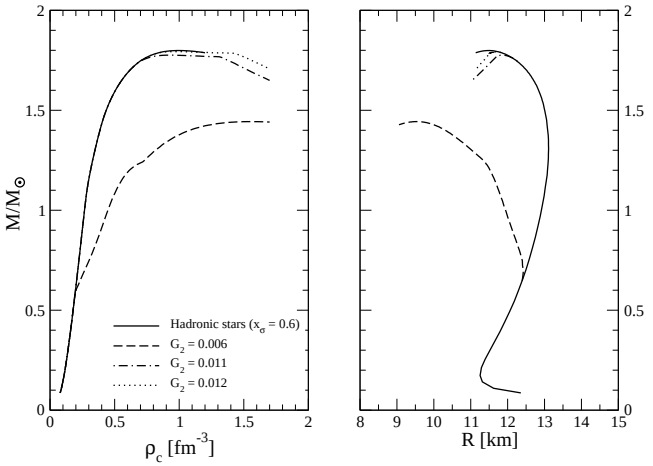


FIG. 9: Same as Fig. 8 but with $x_\sigma = 0.6$.

of calculations for two different sets of the hyperon couplings: one corresponding to $x_\sigma = 0.8$ and the other to $x_\sigma = 0.6$.

In Fig. 8 we plot for the case $x_\sigma = 0.8$ the stellar gravitational mass M versus the central baryon number density ρ_c (left panel) and versus the stellar radius R (right panel), in the case of hyperonic stars (continuous line) and of hybrid stars for different G_2 values. The same quantities are depicted in Fig. 9 for the case $x_\sigma =$

x_σ	G_2	M_{max}	ρ_c^{Hyb}	R	M_{max}^{HS}	ρ_c^{HS}	R^{HS}
	0.006	1.44	1.55	9.54			
N	0.012	1.89	0.77	12.55	2.33	0.87	11.70
	0.016	2.05	0.75	12.66			
	0.006	1.44	1.56	9.52			
0.8	0.012	1.89	0.77	12.53	2.15	0.94	11.50
	0.016	2.04	0.81	12.40			
	0.006	1.43	1.56	9.51			
0.6	0.010	1.73	0.89	12.00	1.80	1.00	11.49
	0.013	1.80	1.00	11.49			

TABLE I: Properties of the maximum mass configuration for hybrid stars for different values of the gluon condensate G_2 in GeV^4 (second column) and for $V_1 = 0.01\,\mathrm{GeV}$. The parameter x_σ (first column) fixes the hyperons coupling constants as described in Sec. III. The entry N in the first column refers to the case of pure nucleonic matter for the hadronic phase. For the case $x_\sigma = 0.6$, hybrid stars are possible only for $G_2 \lesssim 0.013\,\mathrm{GeV}^4$ (see Fig. 11). The mass M_{max}, the central baryon number density ρ_c^{Hyb} and the radius R of the maximum mass configuration are reported respectively in the third, fourth and fifth columns. The quantities with the label HS refer to the case of purely hadronic stars. Stellar masses are reported in units of the solar mass $M_\odot = 1.99 \times 10^{33}$g, central densities are given in fm^{-3}, and stellar radii in km.

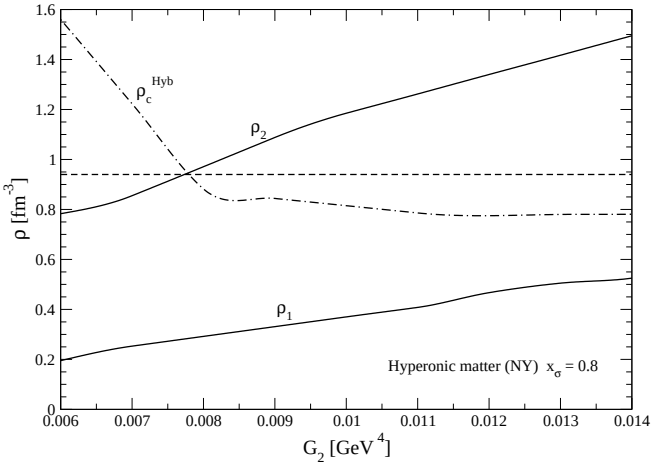


FIG. 10: Quark-hadron phase transition boundaries in β-stable matter as a function of the gluon condensate G_2 and for $V_1 = 0.01\,\mathrm{GeV}$. The onset of quark-hadron mixed phase occurs at the density ρ_1, and the pure quark phase begins at ρ_2. Also shown is the central number density ρ_c^{Hyb} of the maximum mass hybrid star. The horizontal dashed line represents the value of the central density ρ_c^{HS} of the maximum mass pure hadronic star. For the EOS of hadronic phase only nucleons and hyperons (NY) are included with $x_\sigma = 0.8$.

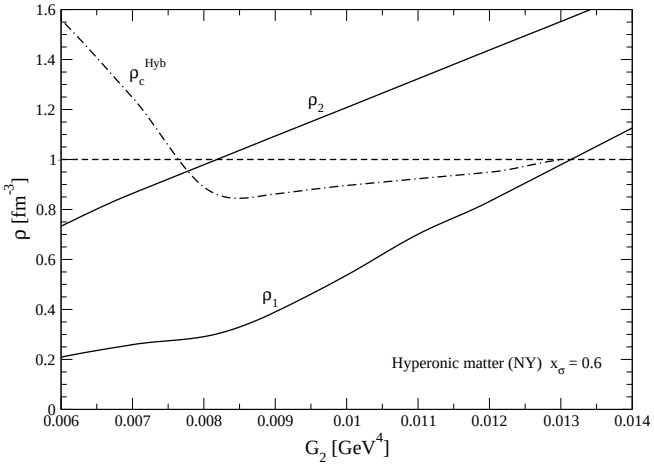


FIG. 11: Same as Fig. 10 but with $x_\sigma = 0.6$.

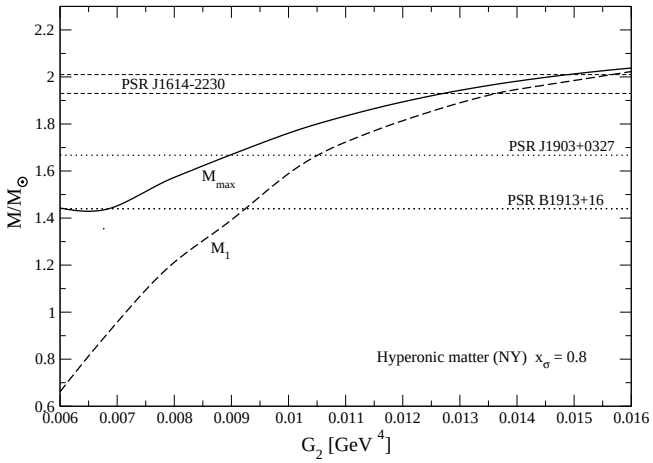


FIG. 12: Gravitational maximum mass for hybrid stars (continuous line) and gravitational mass M_1 (dashed line) of the star with central density ρ_1 corresponding to the onset of mixed quark-hadron phase as a function of the gluon condensate G_2 and for $V_1 = 0.01\,\mathrm{GeV}$. The hadronic phase consists of hyperonic matter (NY) and is described by the GM1 model with $x_\sigma = 0.8$.

0.6. As it is well known [76], the presence of hyperons reduces the value of the maximum mass of pure hadronic star (i.e. compact stars with no quark matter content) from $M_{max} = 2.33\,M_\odot$ in the case of pure nucleonic stars (continuous line in Fig. 5) to $M_{max} = 1.80\,M_\odot$ in the case of hyperonic stars with $x_\sigma = 0.6$ (continuous line in Fig. 9). More interesting is to evaluate the effect of hyperons on the hybrid star sequence as a function of the gluon condensate. As we can see, comparing the results

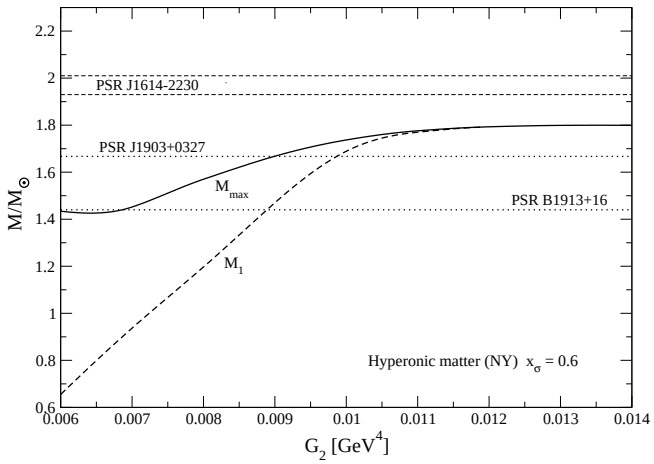


FIG. 13: Same as Fig. 12 but with $x_\sigma = 0.6$.

in Figs. 8 and 9 with those in Fig. 5, for "low" values of the gluon condensate (i.e. $G_2 \lesssim 0.008\,\mathrm{GeV}^4$), the hybrid star sequence is unaffected by the presence of hyperons. In fact, for these low values of G_2 the threshold density for hyperons is larger than the density ρ_1 for the onset of the quark-hadron mixed phase (see Fig. 1).
As in the case of pure nucleonic matter, we obtain stable hybrid star configurations for all the considered values of the gluon condensate and for the two considered sets of hyperon coupling constants. Notice that the hybrid star branch shrinks as G_2 is increased. Additionally, in the case $x_\sigma = 0.6$, hybrid stars are possible only for $G_2 \lesssim 0.013\,\mathrm{GeV}^4$. In fact, for $G_2 \gtrsim 0.013\,\mathrm{GeV}^4$ the baryon number density ρ_1 for the onset of the mixed phase is larger than the central baryon number density ρ_c^{HS} of the maximum mass pure hadronic star (see also Fig. 11).

The properties of the maximum mass configuration for hybrid star sequences varying G_2 and the hyperon coupling constants are summarized in Table I together with those for pure nucleonic and hyperonic star sequences.

We next plot in Fig. 10 (case with $x_\sigma = 0.8$) and in Fig. 11 (case with $x_\sigma = 0.6$) the quark-hadron phase transition boundaries in β-stable matter as a function of G_2. As before (Fig. 6) we denote with ρ_1 (ρ_2) the density for the onset of the quark-hadron mixed phase (pure quark phase). The curve labeled ρ_c^{Hyb} represents the central density of the maximum mass hybrid star. The horizontal dashed line represents the value of the central density ρ_c^{HS} of the maximum mass pure hadronic star (i.e. hyperonic star).

As one can see, comparing the results in Figs. 10 and 11 with those reported in Fig. 6, for "low" values of the gluon condensate (i.e. $G_2 \lesssim 0.008\,\mathrm{GeV}^4$), the densities ρ_1 and ρ_2 are unaffected by the presence of hyperons. When $G_2 \gtrsim 0.008\,\mathrm{GeV}^4$ the inclusion of hyperons produces a sizeable increase of the density ρ_1 and reduces the extension of the range $\rho_2 - \rho_1$ of the mixed phase. In particular, in the case $x_\sigma = 0.6$ (Fig. 11), as we have already pointed out, $\rho_1 > \rho_c^{HS}$ when $G_2 \gtrsim 0.013\,\mathrm{GeV}^4$, thus no deconfinement phase transition occurs in pure hyperonic stars.

The hybrid star maximum mass M_{max} (continuous line) and the mass $M_1 = M(\rho_1)$ (dashed line) as a function of G_2 are plotted in Fig. 12 (case with $x_\sigma = 0.8$) and in Fig. 13 (case with $x_\sigma = 0.6$). From the lower bound of the measured mass of PSR J1614-2230, in the case with $x_\sigma = 0.8$, we obtain $G_2 \gtrsim 0.0127$ GeV^4. Notice that in the case with $x_\sigma = 0.6$, hybrid stars ($G_2 \lesssim 0.013\,\mathrm{GeV}^4$) or pure hyperonic stars ($G_2 \gtrsim 0.013\,\mathrm{GeV}^4$) are not compatible the lower bound of the measured mass of PSR J1614-2230.

To explore the influence of the large-distance static $Q\bar{Q}$ potential V_1 on the stellar properties, we report in Fig. 14 the stellar mass M versus ρ_c (left panel) and M versus R (right panel) in the case of pure nucleonic stars (continuous line) and of hybrid stars for different G_2 values and $V_1 = 0.10\,\mathrm{GeV}$. Once again we get stable hybrid star configurations for all the considered values G_2, with maximum masses ranging from $M_{max} = 2.00\,M_\odot$ (case with $G_2 = 0.006\,\mathrm{GeV}^4$) to $M_{max} = 2.25\,M_\odot$ ($G_2 = 0.0016\,\mathrm{GeV}^4$). Comparing the results in Fig. 14 with those reported in Fig. 5 (case with $V_1 = 0.01\,\mathrm{GeV}$), we clearly see that a larger value of V_1 reduces the extent the hybrid star branch, shifts it to larger densities (see also results in Fig. 2) and produces hybrid stars with a larger maximum mass. Notice that, in this case the calculated M_{max} is compatible with the lower bound of the measured mass of PSR J1614-2230 for all the considered values of the gluon condensate (i.e. $G_2 \gtrsim 0.006\,\mathrm{GeV}^4$).

We also considered stellar models with $V_1 = 0.50\,\mathrm{GeV}$ and $V_1 = 0.85\,\mathrm{GeV}$. For these values of V_1 no phase transition occurs in neutron stars (i.e. $\rho_1 > \rho_c^{HS}$), thus in this case PSR J1614-2230 would be a pure nucleonic star.

Finally to explore the role of the phase transition treatment, we plot in Fig. 15, making use of the Maxwell construction, the stellar gravitational mass M versus ρ_c (left panel) and the mass versus radius R (right panel) in the case of pure nucleonic stars (continuous line) and of hybrid stars for $V_1 = 0.01\,\mathrm{GeV}$ and for three different G_2 values. Stable hybrid stars exist in the case of $G_2 = 0.006\,\mathrm{GeV}^4$ having a maximum mass configuration with $M_{max} = 1.41\,M_\odot$, $\rho_c^{Hyb} = 1.66\,\mathrm{fm}^{-3}$, and $R = 9.35\,\mathrm{km}$. For the other two considered values of the gluon condensate ($G_2 = 0.012\,\mathrm{GeV}^4$ and $0.016\,\mathrm{GeV}^4$) no stable hybrid star can be formed. In fact, an instability develops as soon as the stellar central density equals the critical density for the quark deconfinement transition. These unstable hybrid stars are those represented in Fig. 15 by the decreasing branch of the $M(\rho_c)$ curve and by the configurations on the left of the cusp in the mass-radius curve. The results in Fig. 15 are in agreement

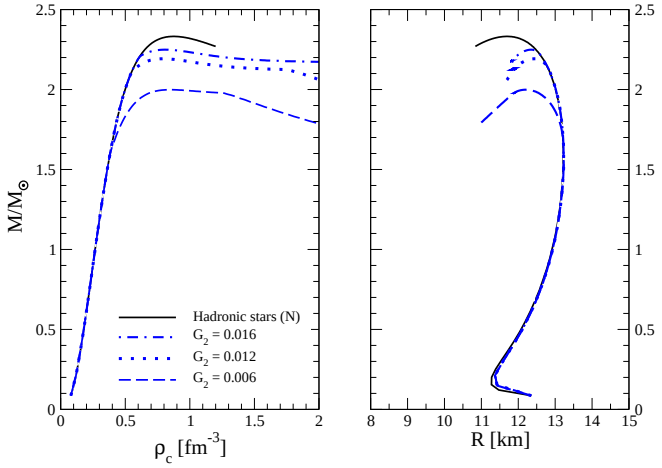


FIG. 14: Same as Fig. 5 but with $V_1 = 0.10\,\mathrm{GeV}$.

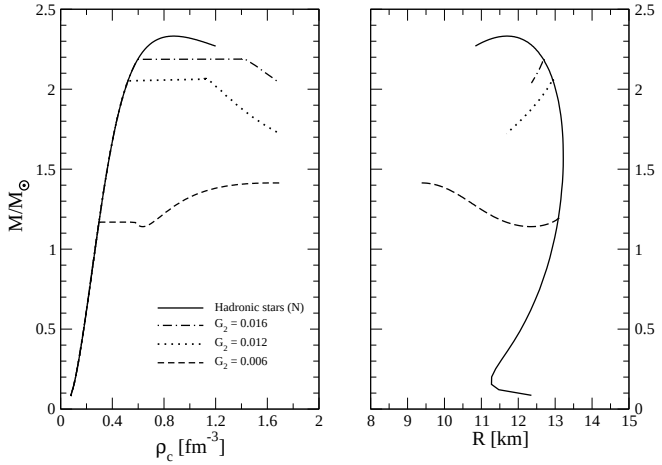


FIG. 15: Same as Fig. 5 but using the Maxwell construction to model the hadron-quark phase transition.

with those reported in Ref. [51] where, making use of the Maxwell construction, stable hybrid star configurations were found only for $0.006\,\mathrm{GeV}^4 < G_2 < 0.007\,\mathrm{GeV}^4$. Thus comparing the results in Fig. 15 with the analogous results in Fig. 5, but obtained using the Gibbs construction, we deduce that the stability of hybrid star equlilibrium configurations within the field correlator method is related to the modeling of the deconfinement phase transition rather than to the confining features of the quark matter model [51]. We have verified that this conclusion is valid also in the case the hadronic phase contains hyperons (NY matter with $x_\sigma = 0.6$ and 0.8).

VI. LATTICE QCD CALCULATIONS AND MEASURED NEUTRON STAR MASSES

Within the FCM the deconfinement transition temperature T_c at $\mu_b = 0$ reads [43]

$$T_c = \frac{a_0}{2} G_2^{1/4} \left(1 + \sqrt{1 + \frac{V_1(T_c)}{2 a_0 G_2^{1/4}}} \right), \qquad (32)$$

with $a_0 = (3\pi^2/768)^{1/4}$ in the case of three flavors. In their analysis the authors of Ref. [43] assume $V_1(T_c) = 0.5\,\mathrm{GeV}$, thus T_c in Eq. (32) is a simple function of G_2 and is represented in Fig. 16 by the curve labeled $V_1(T_c) = 0.5\,\mathrm{GeV}$. This result can hence be compared with lattice QCD calculations of T_c giving the possibility to extract the range of values for the gluon condensate compatible with lattice results. This comparison has been done by the authors of Ref. [43], and it is done in the present work in Fig. 16, where we consider the recent lattice QCD calculations carried out by the HotQCD Collaboration [48] giving $T_c = (154 \pm 9)\,\mathrm{MeV}$ (red continuous lines) and by the Wuppertal-Budapest Collaboration [47] giving $T_c = (147 \pm 5)\,\mathrm{MeV}$ (blue short-dashed lines). As one can see, the comparison with lattice QCD calculations of T_c restricts the gluon condensate in a rather narrow range $G_2 = 0.0025$–$0.0050\,\mathrm{GeV}^4$.

Next to verify if these values of G_2 are compatible with those extracted in Sec. V from hybrid star calculations and measured neutron star masses, we need to relate the parameter $V_1 \equiv V_1(0)$ entering in the zero temperature EOS of the quark phase with $V_1(T_c)$ in Eq.(32). To this end, one can integrate Eq.(4) using the nonperturbative contribution (5) to the color electric correlator $D_1^E(x)$ and assuming that the normalization factor $D_1^E(0)$ does not depend on temperature. The latter assumption is supported, up to temperatures very near to T_c, by lattice calculations [56–58]. Therefore one gets

$$V_1(T) = V_1(0) \left\{ 1 - \frac{3}{2}\frac{\lambda T}{\hbar c} + \frac{1}{2}\left(1 + 3\frac{\lambda T}{\hbar c} \right) e^{-\frac{\hbar c}{\lambda T}} \right\}. \qquad (33)$$

Thus $V_1(T_c) = 0.5\,\mathrm{GeV}$ corresponds to $V_1(0) = 0.85\,\mathrm{GeV}$ to be used in the $T = 0$ EOS of the quark phase. In this case, as we found in Sec. V, no phase transition occurs in neutron stars (i.e $\rho_1 > \rho_c^{NS}$) for all the considered values of G_2. Thus for these values of the EOS parameters PSR J1614-2230 would be a pure nucleonic star.

We can also evaluate the FCM transition temperature at $\mu_b = 0$ corresponding to the case $V_1(0) = 0.01\,\mathrm{GeV}$ used in Sec. V for hybrid star calculations with the $T = 0$ FCM equation of state. To this purpose we solve numerically Eqs. (32) and (33) and we obtain the results represented in Fig. 16 by the curve labeled $V_1 = 0.01\,\mathrm{GeV}$. The comparison of these results with lattice QCD calculations [47, 48] of T_c restricts the gluon condensate in the range $G_2 = 0.0103$–$0.0180\,\mathrm{GeV}^4$. Coming now to the astrophysical constraints on the gluon condensate, the vertical green line in Fig. 16

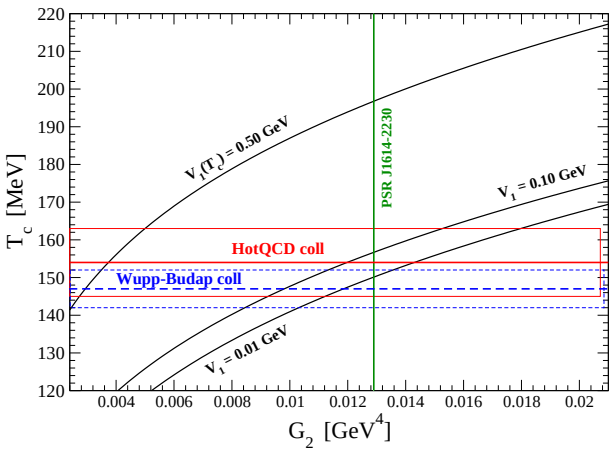


FIG. 16: (color online) Deconfinement transition temperature T_c at $\mu_b = 0$. The curve labeled with $V_1(T_c) = 0.5\,\mathrm{GeV}$ reproduces the FCM results of Ref. [43] for a fixed value $V_1(T_c) = 0.5\,\mathrm{GeV}$ of the large-distance static $Q\bar{Q}$ potential. The curve labeled with $V_1 = 0.01\,\mathrm{GeV}$ ($V_1 = 0.10\,\mathrm{GeV}$) corresponds to the transition temperature at $\mu_b = 0$ obtained solving numerically Eqs. (32) and (33) for the case $V_1(0) = 0.01\,\mathrm{GeV}$ [$V_1(0) = 0.10\,\mathrm{GeV}$]. The horizontal heavy and thin lines represent respectively the central value and the error estimate of lattice QCD calculations. In particular, the (red) continuous lines refer to the calculations [48] of the HotQCD Collaboration $T_c = (154 \pm 9)\,\mathrm{MeV}$; the (blue) short-dashed lines refer to the calculations [47] of the Wuppertal-Budapest Collaboration $T_c = (147 \pm 5)\,\mathrm{MeV}$. Finally, the vertical green line represents the lower limit for G_2 which is compatible with the lower bound of the measured mass of PSR J1614-2230 for the case $V_1(0) = 0.01\,\mathrm{GeV}$.

represents the lower limit for G_2 which is compatible, in the case $V_1(0) = 0.01\,\mathrm{GeV}$, with the lower bound of the measured mass of PSR J1614-2230 (see Sec. V).
A similar analysis can be done for the case $V_1(0) = 0.10\,\mathrm{GeV}$. Now the comparison between the FCM transition temperature at $\mu_b = 0$ (curve labeled $V_1 = 0.10\,\mathrm{GeV}$ in Fig. 16) and lattice QCD calculations of the same quantity gives $G_2 = 0.0085$–$0.0153\,\mathrm{GeV}^4$, whereas one gets $G_2 \geq 0.006\,\mathrm{GeV}^4$ from the lower bound of the measured mass of PSR J1614-2230.

We thus find that the values of the gluon condensate extracted within the FCM from lattice QCD calculations of the deconfinement transition temperature at zero baryon chemical potential are compatible with the value of the same quantity extracted from measured neutron star masses.

VII. SUMMARY AND CONCLUSIONS

In this article we have studied the hadron-quark deconfinement phase transition in β-stable matter and the structural properties of hybrid stars using an EOS for the quark phase derived from the field correlator method extended to finite baryon chemical potential. This EOS model was parametrized in terms of the gluon condensate G_2 and of the large-distance static $Q\bar{Q}$ potential V_1 at zero temperature. For the hadronic phase we utilized the GM1 parametrization of the nonlinear relativistic mean field model, and we have considered pure nucleonic matter as well as hyperonic matter with a large hyperon fraction (x_σ=0.6), and a small hyperon fraction ($x_\sigma = 0.8$).

We found that increasing the value of the gluon condensate G_2 caused a shift of the phase transition to larger baryon densities. Moreover, for the case $V_1 = 0.01\,\mathrm{GeV}$, when $G_2 \gtrsim 0.008\,\mathrm{GeV}^4$ the inclusion of hyperons produced a considerable increase of the mixed phase onset density ρ_1 and reduced the extension of the range $\rho_2 - \rho_1$ of the mixed phase. In particular, in the case $x_\sigma = 0.6$, when $G_2 \gtrsim 0.013\,\mathrm{GeV}^4$ no deconfinement phase transition occurred in pure hyperonic stars.

Applying the Gibbs construction to model the phase transition, we obtained stable hybrid star configurations for all the values of the gluon condensate fulfilling the condition $\rho_1(G_2) < \rho_c^{HS}(G_2)$ (i.e. the deconfinement transition can occur in pure hadronic stars). We found that the hybrid star branch shrank as G_2 was increased.

We have established that the values of the gluon condensate extracted within the FCM from lattice QCD calculations of the deconfinement transition temperature at $\mu_b = 0$ were consistent with the value of the same quantity derived by the mass measurement of PSR J1614-2230. The FCM thus provides a powerful tool to link numerical calculations of QCD on a space-time lattice with neutron stars physics.

[1] J. M. Lattimer and M. Prakash, Astrophys. J. **550**, 426 (2001).
[2] G. X. Peng, A. Li, and U. Lombardo, Phys. Rev. C **77**, 065807 (2008).
[3] Z. H. Li and H.-J. Schulze, Phys. Rev. C **78**, 028801 (2008).
[4] I. Vidaña, D. Logoteta, C. Providência , A. Polls, and I. Bombaci, Europhys. Lett. **94**, 11002 (2011).
[5] M. G. Alford, A. Schmitt, K. Rajagopal, and T. Schafer, Rev. Mod. Phys. **80**, 1455 (2008).
[6] F. Weber, Prog. Part. Nucl. Phys. **54**, 193 (2005).
[7] M. Prakash, I. Bombaci, M. Prakash, P. J. Ellis, J. M. Lattimer and R. Knorren, Phys. Rep. **280**, 1 (1997).
[8] I. Bombaci, Eur. Phys. J. A **31**, 810 (2007).
[9] M. A. Perez-Garcia, J. Silk, and J. R. Stone, Phys. Rev. Lett. **105**, 141101 (2010).

[10] H. Sotani, N. Yasutake, T. Maruyama, and T. Tatsumi, Phys. Rev. D **83**, 024014 (2011).

[11] Z. Berezhiani, I. Bombaci, A. Drago, F. Frontera, and A. Lavagno, Astrophys. J. **586**, 1250 (2003); I. Bombaci, I. Parenti, and I. Vidaña, Astrophys. J. **614**, 314 (2004).

[12] G. Lugones and I. Bombaci, Phys. Rev. D **72**, 065021 (2005); I. Bombaci, G. Lugones, and I. Vidaña, Astron. Astrophys. **462**, 1017 (2007).

[13] I. Bombaci, D. Logoteta, P.K. Panda, C. Providência, and I. Vidaña, Phys. Lett. B **680**, 448 (2009); I. Bombaci, D. Logoteta, C. Providência, and I. Vidaña, Astron. and Astrophys. **528**, A71 (2011).

[14] D. Logoteta, C. Providência, I. Vidaña, and I. Bombaci, Phys. Rev. C **85**, 055807 (2012).

[15] S. Weissenborn, I. Sagert, G. Pagliara, M. Hempel, and J. Schaffner-Bielich, Astrophys. J. **740**, L14 (2011).

[16] N. Nishimura, T. Fischer, F.-K. Thielemann, C. Fröhlich, M. Hempel, R. Käppeli, G. Martnez-Pinedo, T. Rauscher, I. Sagert, and C. Winteler, Astrophys. J. **758**, 9, (2012).

[17] C. Bernard, T. Burch, C. DeTar, J. Osborn, S. Gottlieb, E. B. Gregory, D. Toussaint, U. M. Heller, and R. Sugar, Phys. Rev. D **71**, 034504 (2005).

[18] M. Cheng et al., Phys. Rev. D **74**, 054507 (2006).

[19] Y. Aoki, G. Endrodi, Z. Fodor, S. D. Katz, and K. K. Szabó, Nature (London) **443**, 675, (2006).

[20] M. P. Lombardo, J. Phys. G **35** 104019 (2008); Proc. Sci LATTICE2012 (2012) 016 [arXiv:1301.7324].

[21] E. Farhi and R. L. Jaffe, Phys. Rev. D **30**, 272 (1984).

[22] A. Chodos, R. L. Jaffe, K. Johnson, C. B. Thorn and V.F. Weisskopf, Phys. Rev. D **9**, 3471 (1974).

[23] E. Witten, Phys. Rev. D **30**, 272 (1984).

[24] C. Alcock, E. Farhi, and A. Olinto, Astrophys. J. **310**, 261 (1986).

[25] P. Haensel, J. L. Zdunik, and R. Schaeffer, Astron. Astrophys. **160**, 121 (1986).

[26] X.-D. Li, I. Bombaci, M. Dey, J. Dey, and E.P.J. van den Heuvel, Phys. Rev. Lett., **83**, 3776 (1999); X.-D., Li, S. Ray, J. Dey, M. Dey, and I. Bombaci, Astrophys. J. **527**, L51 (1999).

[27] R. X. Xu, G. J. Qiao, and B. Zhang, Astrophys. J. **522**, L109 (1999).

[28] B. A. Freedman and L. D. McLerran, Phys Rev. D **16**, 1130 (1977); **17**, 1109 (1978).

[29] V. Baluni, Phys Rev. D **17**, 2092 (1978).

[30] A. Kurkela, P. Romatschke, and A. Vuorinen, Phys Rev. D **81**, 105021 (2010).

[31] Y. Nambu and Jona-Lasinio, Phys Rev. **122**, (1961) 345.

[32] M. Buballa, Phys. Rep. **407**, 205 (2005).

[33] U. Vogland, and W. Weise, Prog. Part. Nucl. Phys. **27**, 195 (1991).

[34] S.P. Klevansky, Rev. Mod. Phys **64**, 649 (1992).

[35] T. Hatsuda and T. Kunihiro, Phys Rep. **247**, 221 (1994).

[36] O. Benhar and A. Cipollone, Astron. Astrophys. **525** L1 (2011).

[37] K. Schertler, S. Leupold, and J. Schaffner-Bielich, Phys. Rev. C **60**, 025801 (1999).

[38] M. Buballa, F. Neumann, M. Oertel, and I. Shovkovy, Phys. Lett. B **595**, 36 (2004).

[39] F. Yang, and H. Shen, Phys. Rev. C **77**, 025801 (2008).

[40] D. Logoteta, I. Bombaci, C. Providência, and I. Vidaña, Phys. Rev. D **85**, 023003 (2012).

[41] H. G. Dosch, Phys. Lett. B **190**, 177 (1987); H. G. Dosch, and Y. Simonov, Phys. Lett. B **205**, 339 (1988); Y. Simonov, Nucl. Phys. B **307**, 512 (1988).

[42] A. Di Giacomo, H. G. Dosch, V. I. Shevchenko and Y. A. Simonov, Phys. Rep **372**, 319 (2002).

[43] Y. A. Simonov, and M. A. Trusov, JETP Lett. **85**, 598 (2007); Y. A. Simonov, and M. A. Trusov, Phys. Lett. B **650**, 36 (2007).

[44] Y. A. Simonov, Phys. Lett. B **619**, 293 (2005).

[45] Y. A. Simonov, Ann. Phys. **323**, 783 (2008).

[46] A. V. Nefediev, Y. A. Simonov, and A. M. Trusov, Int. J. Mod. Phys. E **18**, 549 (2009).

[47] S. Borsanyi et al, J. High Energy Phys. **09**, 073 (2010).

[48] A. Bazavov et al, Phys. Rev. D **85**, 054503 (2012).

[49] J.D. Walecka, Ann. Phys. (N.Y.) **83**, 491 (1974); B.D. Serot, and J.D. Walecka, Adv. Nucl. Phys. **16**, 1 (1986).

[50] J. Boguta, and A. R. Bodmer, Nucl. Phys. A **292**, 413 (1977).

[51] M. Baldo, G. F. Burgio, P. Castorina, S. Plumari, and D. Zappalà Phys. Rev. D **78** 063009 (2008).

[52] M. Baldo, I. Bombaci, and G.F. Burgio, Astron. Astrophys. **328**, 274 (1997).

[53] M. Baldo, I. Bombaci, G. Giansiracusa, U. Lombardo, C. Mahaux, and R. Sartor, Phys. Rev. C **41**, 1748 (1990).

[54] Z. H. Li, U. Lombardo, H.-J. Schulze, W. Zuo, L.W. Chen, and H.R. Ma, Phys. Rev. C **74**, 047304 (2006).

[55] F. I. M. Pereira, Nucl. Phys. A**860** 102 (2011); Nucl. Phys. A**897** 151 (2013).

[56] A. Di Giacomo and H. Panagopoulos, Phys. Lett. B **285**, 133 (1992).

[57] M. D' Elia, A. Di Giacomo, and E. Meggiolaro, Phys. Lett. B **408**, 315 (1997).

[58] E. Meggiolaro, Phys. Lett. B **451**, 414 (1999); M. D' Elia, A. Di Giacomo, and E. Meggiolaro, Phys. Rev. D **67**, 114504 (2003).

[59] Y. A. Simonov, Phys. At. Nucl. **61**, 855 (1998); H. G. Dosch, M. Eidemuller, and M Jamin, Phys. Lett. B **452**, 379 (1999); Y. A. Simonov, Phys. At. Nucl. **69**, 528 (2006).

[60] M. Doring, S. Ejiri, O. Kaczmarek, F. Karsch, and E. Laermann, Eur. Phys. J. **C46**, 179 (2006).

[61] M. A. Shifman, A. I. Vainshtein, and V. I. Zakharov, Nucl. Phys. **B147**, 385 (1979); Nucl. Phys. **B147**, 448 (1979).

[62] A. Di Giacomo, E. Meggiolaro, Y. Simonov, and A. I. Veselov, Phys. At. Nucl. **70**, 908 (2007).

[63] N.K. Glendenning and S. Moszkowski, Phys. Rev. Lett. **67**, 2414 (1991).

[64] N. K. Glendenning, *Compact Stars, Nuclear Physics, Particle Physics, and General Relativity* (Springer, New York, 2000), 2nd ed.

[65] I. Bombaci, P.K. Panda, C. Providência, and I. Vidaña, Phys. Rev. **D77**, 083002 (2008).

[66] Z. Fodor and S. D. Katz, J. High Energy Phys. 04 (2004) 050.

[67] N.K. Glendenning, Phys. Rev. D **46**, 1274 (1992).

[68] D. N. Voskresensky, M. Yasuhira, and T. Tatsumi, Nucl. Phys. A **723**, 291 (2003).

[69] T. Maruyama, S. Chiba, H.-J. Schulze, and T. Tatsumi, Phys. Rev. D **76**, 123015 (2007)

[70] A. Bhattacharyya, I. N. Mishustin, and W. Greiner, J. Phys. G **37**, 025201 (2010).

[71] P. Haensel, A. Y. Potekhin, and D. G. Yakovlev, *Neutron Stars 1: Equation of State and Structure* (Springer, New York, 2007).

[72] G. Baym, C. Pethick, and D. Sutherland, Astrophys. J.

170, 299 (1971); J. W. Negele, and D. Vautherin, Nucl. Phys. A **207**, 298 (1973).
[73] R. A. Hulse and J. H. Taylor, Astrophys J. **195** (1975) L51; J. M. Weisberg, D. J. Nice, and J. H. Taylor, Astrophys J. **722**, 1030 (2010).
[74] P. C. C. Freire et al., Mont. Not. R. Astron. Soc. **412**, 2763 (2011).
[75] P. Demorest, T. Pennucci, S. Ransom, M. Roberts, and J. Hessels, Nature (London) **467**, 1081 (2010).
[76] N.K. Glendenning, Astrophys. J. **293**, 470 (1985).
[77] For a detailed discussion of the differences between the Maxwell and the Gibbs phase transition constructions including the effects of surface tension and electromagnetic energy see Ref. [68, 69].